The Study of Hydrothermal Carbonization and Activation Factors' Effect on Mesoporous Activated Carbon Production from *Sargassum* sp. Using a Multilevel Factorial Design

Tirto Prakoso[1,2,*)], Heri Rustamaji[1,3)], Daniel Yonathan[1)], Jenny Rizkiana[1,2)], Hary Devianto[1)], Pramujo Widiatmoko[1)], and Guoqing Guan[4)]

[1]Department of Chemical Engineering, Faculty of Industrial Technology, Bandung Institute of Technology,
Bandung 40132 Indonesia
[2]Department of Bioenergy Engineering and Chemurgy, Faculty of Industrial Technology,
Bandung Institute of Technology,
Bandung 40132 Indonesia
[3]Department of Chemical Engineering, Lampung University,
Bandar Lampung 35145 Indonesia
[4] Section of Renewable Energy, Institute of Regional Innovation, Hirosaki University,
Aomori 036-8561 Japan

[*)] Corresponding author: tirto@che.itb.ac.id

Abstract

Seaweeds are large-scale multicellular marine algae categorized based on color as Chlorophyceae, Rhodophyceae, and Phaeophyceae. No information has been provided on the conditions affecting the production of mesoporous activated carbon from one member of the described aquatic plants, Sargassum sp. Therefore, this study aimed to determine the impact of the main factors and their interactions on Sargassum sp.-derived activated carbon manufactured (SAC) by hydrothermal carbonization and CO_2 activation methods. A mathematical approach was employed using a multilevel factorial design with the main factors being the activator type ($ZnCl_2$, $CaCl_2$, & KOH), hydrothermal temperature (200, 225, & 250ºC), and activator ratios (2 & 4). Meanwhile, the response variables were yield and BET surface area (S_{BET}) of SAC. Morphological, functional, crystallographic, and porosity characterization was carried out on the samples. The SAC-Ca-200-2 sample had the highest yield, with the value of 26.5 percent of weight. The activators having the highest specific surface area (S_{BET}) were SAC-Zn-250-4, SAC-Ca-225-2, and SAC-K-250-2, with 1552, 1368, and 1799 m^2/g, respectively. The pore size distribution in SAC products ranged from 2.16 to 10 nm in diameter. The analysis conducted indicated that the activator type and interaction with its ratio substantially impacted the SAC yield value; besides, only the activator type affects the formation of high surface area pores.

Keywords: *Hydrothermal carbonization, activation, Sargassum sp.-based activated carbon, multilevel factorial design, statistical analysis*

INTRODUCTION

Seaweeds are large-scale multicellular marine algae (Xu et al., 2013) that are categorized into three types based on their color, namely green (*Chlorophyceae*), red (*Rhodophyceae*), and brown (*Phaeophyceae*), macroalgae (Brown et al., 2020). These three are found in Indonesia, with red algae most abundant in the public water bodies. Although seaweed is harvested worldwide, eight countries in Asia produce nearly 97.26% of the total quantity recorded in 2019. According to the Food and Agriculture Organization (FAO), China controls 65.7 % of the total production of 30.05 million tons, while Indonesia controls 27.8 %, making both the primary producers (Cai et al., 2021). Seaweed is versatile, therefore used as a fertilizer, food additive, and animal feed ingredient or separated for carbohydrates such as gelatin or carrageenan. However, 80 % of Indonesian seaweed exports are still low-added value material among the dried forms shipped from China, South Korea, and Vietnam (Saleh and Sebastian, 2020).

Converting seaweed into biochemicals, biofuels, and biomaterials increases the added value. Biofuel and biomaterials synthesis in biochar and activated carbon form from various kinds of this plant have been investigated in previous studies using hydrothermal carbonization and pyrolysis methods. Li et al. (2011) studied the processing kinetics of three types of red algae. They identified three steps of the pyrolysis process: water evaporation, initial devolatilization, and lingering transformation. Kim et al. (2013) studied the properties of thermogravimetry and kinetic parameters of pyrolysis of *Sargassum* sp. at 350ºC. They found that the lumped model approximated the kinetics and the reaction rate to form liquid products rather than gas. Smith and Ross (2016) investigated the monsoon variation of seaweed on the compositional effects of the fuel grade of solid with the HTC process. They showed that the most significant energy yields were harvested in the summer and the fall of algae. Ali and Bahadar (2017) investigated the pyrolysis and devolatilization kinetics of red seaweed at 480-950ºC and found that the lignin component determines the limiting rate. Pintor et al. (2013) synthesized activated carbon by direct pyrolysis for supercapacitor electrodes. The same thing was done by Pourhosseini et al. (2017), who stated that activated carbon from seaweed was promising for supercapacitor electrode material. Zeng et al. (2018) studied activated carbon bonding with a hydrothermal process and activation with a KOH catalyst. The activated carbon produced has a micropore structure and is suitable for CO_2 adsorbent. Perez-Salcedo et al. (2020) synthesized activated carbon by pyrolysis and activation with KOH. The activated carbon produced has a microporous structure with an area of 1493 m^2/g and is suitable for application for electrocatalytic oxygen reduction materials.

Various factors, such as the type of activator, its ratio to biomass, and the hydrothermal carbonization temperature, affect the yield and characteristics of activated carbon. Previous seaweed hydrothermal studies only used KOH activators and had not discussed the effect of using other activating agents such as $ZnCl_2$ and $CaCl_2$. Meanwhile, research on hydrothermal seaweed carbonization by Rustamaji et al. (2022a) with a ChCl catalyst emphasizes the study of the synthesis of the composition of the liquid product (bio-oil). It is limited to the characteristics of hydrochar, which has not yet produced activated carbon. In addition, the pretreatment process with deashing, which will affect the quantity and quality of the product, was not carried out in this study. No information has been reported regarding the synthesis of activated carbon from *Sargassum* sp. with variations of the factors mentioned above, so various experiments are essential to be carried out.

This study examines the properties of activated carbon from the hydrothermal process of seaweed using KOH, $ZnCl_2$, and $CaCl_2$ as activating agents and prior to activation with CO_2. An investigation of the effect of different operational conditions on the characteristics of activated carbon was also carried out. Finally, using the stratified factorial design method and analysis of variance (ANOVA), it was found that the type of activator was the most influential factor in the yield and characteristics of activated carbon. This is followed by the interaction between the type of activator and the ratio of activators to biomass that significantly affect the yield of activated carboned.

RESEARCH METHOD
Materials

Seaweed (*Sargassum* sp.) as the sample was obtained from Jepara, Central Java, dried at 105 ºC for 24 hours, ground, and screened to 40 mesh-sized granules. Zinc chloride ($ZnCl_2$, Merk, p.a), calcium chloride ($CaCl_2$, Merk, p.a), and potassium hydroxide (KOH, Merk, p.a) were used as activators. Hydrochloric acid (HCl, Merck p.a.) and N_2 & CO_2 (99.99%) were purchased from Bratachem Ltd. and Aneka Gas Ltd. in Indonesia.

Preparation of Activated Carbon

The production of activated carbon involves a two-stage procedure, hydrothermal carbonization (HTC) and activation of hydrochar with a CO_2 (Jain et al., 2016; Rustamaji et al., 2022b). The HTC process was carried out by inserting 10 grams of *Sargassum* sp. and activators (concentration= 20 %wt) into a stainless-steel reactor. The ratio of each activator ($ZnCl_2$, $CaCl_2$, and KOH) to the seaweed varied from 2 and 4. Furthermore, the reaction lasted for 60 minutes with temperature variations of 200, 225, and 250ºC. The reactor used was naturally decreased to ambient temperature. The gas product was released into the sampling bag. The product obtained was

filtered with a vacuum filter to separate into a solid and a liquid fraction. The solid product was rinsed with demineralized water until neutral and continued by drying in an oven at 105 °C for 24 hours. The *Sargassum* sp.-derived hydrochar product was denoted as SHC-A-B-C, where A represents the activator, B is the hydrothermal temperature, and C is the ratio of activator to the seaweed.

Hydrochar was activated in a horizontal cylinder reactor. The temperature was increased at a thermal rate of 10 C/min until 800 ºC was reached by flowing N_2 gas at the volume rate of 50 mL/min. At this point, the activation temperature was maintained for two hours by replacing the N_2 stream with CO_2 at 50 ml/min. After activation, the furnace was chilled to room temperature. The product was immersed with 0.1 M HCl for 30 minutes, followed by demineralized water until neutral, then heated in an oven at 105 ºC for 24 hours (Zeng et al., 2018). *Sargassum* sp-derived activated carbon is denoted as SAC-A-B-C with the A, B, and C marked above.

Characterization

Several methods were employed to characterize the samples; hence the ultimate analysis was carried out at the tekMIRA Coal Testing Laboratory in Bandung to determine the elemental content of the biomass. Scanning Electron Microscopy (SEM) analyzed the activated carbons' morphology using SEM Hitachi SU3500 at the Chevron UPP SEM-EDS Laboratory, Bandung Institute of Technology. The infrared spectrum of the model was obtained using a Nicolet 6700 FTIR spectrometer in the wavenumber range of 5000–400 1/cm. The crystallography of the samples was examined using a PANalytical XPert PRO diffractometer with Cu-Kα radiation (40 kV, 40 mA) at the Center for Nanoscience and Nanotechnology Research Bandung Institute Technology.

Moreover, the porosity properties of activated carbon were analyzed with Quantochrome Instruments Nova 3200e at the Chemical Engineering Instrumentation Laboratory, Bandung Institute of Technology. Brunauer-Emmett-Teller (BET) method was applied to calculate the specific surface area of SAC, and the total pore volume was decided at a relative pressure (P/P_0) of about 0.99. Finally, the pore size distribution of the sample was determined using the BJH method (Inagaki and Kang, 2014).

Multilevel Factorial Design

The multilevel factorial design was used to examine all factors at once, and the mathematical model was derived through the ANOVA tables obtained (Özbay et al., 2013). Optimal conditions were determined by involving several factors and varying their levels. In this study, the three used were activator type (A), hydrothermal temperature, and the ratio of the activator to *Sargassum* sp. The respective levels were provided in Table 1 to investigate their

impact on the yield and specific surface area of activated carbon. The yield of SAC was calculated from equation (1):

$$Y = \frac{M_{SAC}}{M_{biomass}} \cdot 100\% \qquad (1)$$

where M_{SAC} was the mass of SAC in grams obtained after the activation process and $M_{biomass}$ was the mass of *Sargassum* sp. fed into the hydrothermal reactor.

Table 1. Factors and levels for experimental design

Factor	Level		
	1	2	3
Activator, A	$ZnCl_2$	$CaCl_2$	KOH
Temperature, B	200	225	250
Activator ratio, C	2	4	

RESULTS AND DISCUSSION
Characterization of Materials
Elemental analysis

The elemental analysis results for *Sargassum* sp.-derived hydrochar (SHC) and SAC can be seen in Table 2. The seaweeds' high carbon content indicated that it was suitable for the synthesis of activated carbon. The carbon concentration expanded altogether while oxygen diminished in the sample Completing the activation procedure, demonstrating the higher carbonaceous content of activated carbon than *Sargassum* sp. and hydrochar (Hoekman et al., 2011). The H/C atomic ratio in seaweed dropped from 0.2 to 0.13 for hydrochar and 0.02 for activated carbon, respectively. Meanwhile, the O/C atomic ratio in this plant fell from 2.68 to 1.2 for hydrochar and 0.29 for activated carbon, respectively, which was generally identified with dehydration, decarboxylation, and de-methanation responses. The two proportions gradually coincided with all home events examined (Gao et al., 2016).

Functional group analysis

Surface functional groups, including oxygen and nitrogen, were identified using Fourier Transforms Infrared Spectroscopy (FTIR). The FTIR spectra of activated carbon can be seen in Figure 1. Based on Figure 1, various activators have different transmittance (inverse of absorbance) even though their functional groups are relatively similar. Furthermore, it showed activated carbon with transmittance arranged sequentially from the smallest to the largest for $ZnCl_2$, $CaCl_2$, and KOH. The O-H stretching vibration in hydroxyl and carboxyl groups was blamed for the peak at 3429 cm^{-1}. The dip at approximately 2368-2370 cm^{-1} corresponds to a C≡C stretch. The absorbance peaks indicate the stretching of C=O in ketone, amide, and carboxylic groups at 1583 cm^{-1}. (Gao et al., 2016).

Table 2. Elemental analysis of *Sargassum* sp., SHC, and SAC

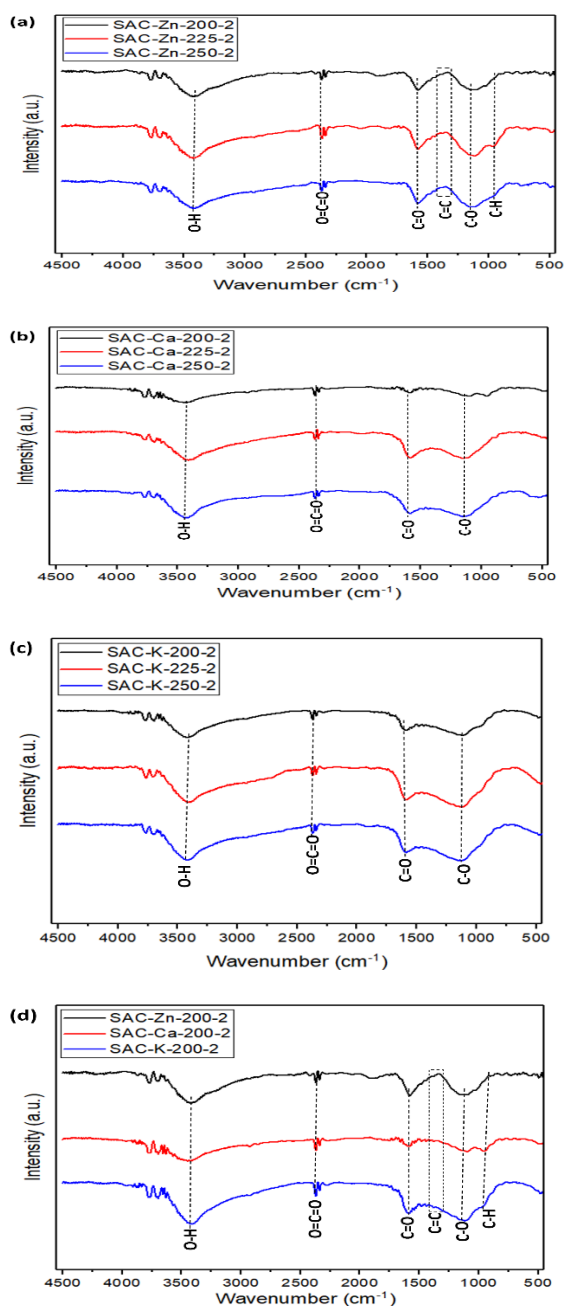| Sample	C (%wt)	H (%wt)	N (%wt)	O (%wt)	S (%wt)	H/C (atomic ratio)	O/C (atomic ratio)
Sargassum sp.	21.11	4.26	0.35	56.73	2.9	0.2	2.68
SHC-Zn-200-2	37.80	5.10	1.40	46.20	1.40	0.13	1.20
SAC-Zn-200-2	73.95	2.13	2.22	21.80	1.82	0.02	0.29

Figure 1. FTIR spectra of activated carbon with different temperatures with activator (a) $ZnCl_2$, (b) $CaCl_2$, (c) KOH, and (d) at various activator

The peak at 1111-1120 cm^{-1} was attributed to the aliphatic ether C-O and phenol C-O stretching, while the characteristic bands at 966 cm^{-1} are ascribed to aromatic C–H out-of-plane bending vibrations (Zhang et al., 2012).

Meanwhile, Figure 1. a-b shows the spectrum of the functional group of activated carbon at various activators and temperatures, with the ratio of the activators to seaweed being 2. It also shows that the difference in hydrothermal carbonization temperature causes a slight difference in the transmittance of the functional groups, which are relatively similar to the activated carbon. According to Wang et al. (2018), hydrochar formation from lignocellulose precursors includes hydrolysis, dehydration/fragmentation, condensation, and polymerization to form polyaromatic and polyfurantic structures. This process will produce several functional groups in the hydrochar product. Saha et al. (2019) analyzed the relative transmittance area percentage (RTAP) of each IR spectrum of hydrochar from wood to evaluate how handling affects peak intensities. The analysis results show that in the temperature range of 180-250 ºC, RATP is not significantly different. At a temperature of 260 ºC, there are RTAP and different types of functional groups. This difference is because, at a temperature of 260 ºC, it begins to enter the liquefaction regime, which produces more liquid products and gaseous CH_4. Activated carbon produced from the activation pyrolysis of hydrochar at a temperature of 800 ºC will have a different functional group intensity from hydrochar; however, the difference in hydrothermal temperature treatment does not cause a significant difference in the functional group of activated carbon. So, the trend of FTIR intensity in this study matches the results of the research by Saha et al. (2019).

Functional groups with an oxygen atom in compounds such as alcohols, ethers, aldehydes, ketones, carboxylic acids, amides, esters, and acid halides are called oxygenated functional groups (OFGs), which are believed to have an adsorption effect on activated carbon; hence Sun *et al.* conducted several studies to increase OFG on this product. The results showed that increasing the amount of oxygenated functional groups elevates the adsorption efficiency (Sun et al., 2017). In addition, OFG improves the wettability, conductivity, and pore size distribution of activated carbon while being an essential factor for manufacturing supercapacitors (He

et al., 2018). Based on Figure 1d, in the three types of activated carbon with different activators, each of the products has a different intensity of O-H, C=O, dan C-O, with activated carbon produced from activating agent of KOH having the highest intensity. In contrast, material with activating agent $ZnCl_2$ produces C-H functional groups. In addition, at wave numbers 1000-1500 cm^{-1}, there is a sharp peak among the three samples, which can be attributed to aromatic ring stretching vibration C=C on activated carbon produced from activating agent of $ZnCl_2$ (Titirici, 2013).

A high concentration of O-H and C-O is very suitable to be used as a material for manufacturing supercapacitors and heavy metal adsorbents. The presence of many O-H and C-O groups is due to the hydrothermal process increasing OFG on hydrochar and activated carbon (Jain et al., 2016). This does not apply to activated carbon produced through conventional methods.

Morphological characterization

The morphology of activated carbon was analyzed using Scanning Electron Microscope (SEM) and Energy Dispersive Spectroscopy (EDS). Morphological characterization was carried out using 500 and 1000x magnification, while characterization of elemental composition was used to determine the contained elements. The SEM results can be seen in Figure 2, showing SAC's pore opening with temperature variations of 200, 225, and 250°C. At 200°C, the pores are still not fully formed compared to 225°C and 250°C.
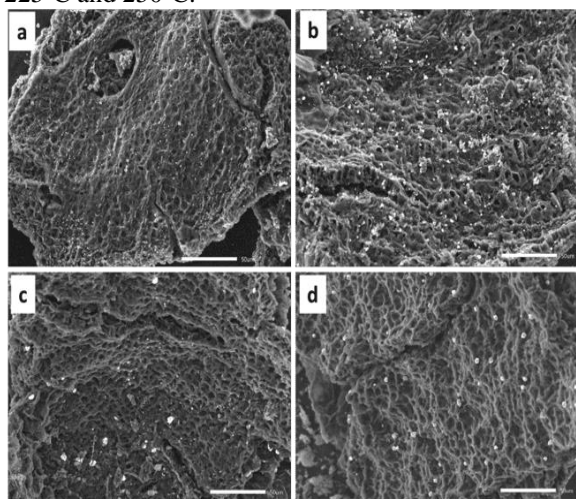

Figure 2. SEM analysis of sample (a) SAC-Zn-200-2, (b) SAC-Zn-225-2, (c) SAC-Zn-250-2, and (d) SAC-Zn-250-4

Titirici et al. (2015) found that the pores on the activated carbon surface tend to be more open and regular while increasing temperature. This opening is caused by an activator that functions as a decomposer of the carbon structure during the carbonization and activation process. At the time of activation with CO_2,

the gaps in the carbon structure filled with materials decomposed during the hydrothermal carbonization were released, thereby opening the seaweed pores. Meanwhile, the activated carbon with $ZnCl_2$, $CaCl_2$, & KOH and an activator ratio of 4 provided a more uniform pore size than 2 (Titirici et al., 2015).

Porosity characterization

Experimental design, yield, and textural properties of SAC, including BET surface area (S_{BET}), total pore volume (V_{total}), and mean pore diameter (d_{av}), are listed in Table 3.

Table 3. Design experiment, yield and textural properties of SAC

Run	Sample SAC	Yield (% wt.)	S_{BET} (m^2/g)	V_{total} (cm^3/g)	d_{av} (nm)
1	SAC-Zn-200-2	14.7	1071	0.58	2.16
2	SAC-Zn-225-2	15.8	1247	0.73	2.34
3	SAC-Zn-250-2	11.9	1450	0.78	2.17
4	SAC-Zn-200-4	21.0	1311	0.87	2.24
5	SAC-Zn-225-4	19.3	1324	0.73	3.01
6	SAC-Zn-250-4	20.5	1552	0.93	2.81
7	SAC-Ca-200-2	26.6	1333	0.83	2.44
8	SAC-Ca-225-2	22.6	1368	0.98	2.96
9	SAC-Ca-250-2	27.2	454	0.47	12.13
10	SAC-Ca-200-4	23.6	447	2.76	7.51
11	SAC-Ca-225-4	20.2	415	1.07	10.36
12	SAC-Ca-250-4	19.4	594	1.51	10.19
13	SAC-K-200-2	6.0	1198	1.14	2.54
14	SAC-K-225-2	5.7	1311	0.82	2.50
15	SAC-K-250-2	5.2	1799	1.00	3.31
16	SAC-K-200-4	7.4	1121	0.79	2.83
17	SAC-K-225-4	12.2	1264	0.90	2.85
18	SAC-K-250-4	15.5	1269	0.86	2.72

The yield was calculated from equation (1) as all samples were activated at 800°C. At the same time, at the appropriate hydrothermal temperature, SAC-K-250-2 produced the largest specific surface area with a value of 1799 m^2g^{-1} but with the lowest yield. This was probably because the KOH activator triggered the free carbon reaction with CO_2 and the evaporation of volatiles at 800°C to ensure the carbon produced was low.

The N_2 sorption isothermal examination was also used to explore the activated carbon sample's structure. The isotherms for nitrogen adsorption at -196°C for the chemically activated carbon prepared using different activators can be seen in Figure 3.a. The curve shows a type IV isotherm with a kind IV hysteresis loop (per IUPAC classification), while the N_2 adsorption mainly occurs at a relative pressure range from 0.4 to 1.0. Type IV isotherms indicate the existence of well-developed mesopores in the structure. In contrast, a kind IV hysteresis loop

suggests the development of asymmetric, cut-form mesopores, owing to fast gas advancement and open channels (Yang et al., 2012; Hossain et al., 2018). Generally, the shape of the isotherms changes with a different activator because of an increase in the volume of nitrogen adsorbed by $ZnCl_2$, $CaCl_2$, and KOH, respectively.
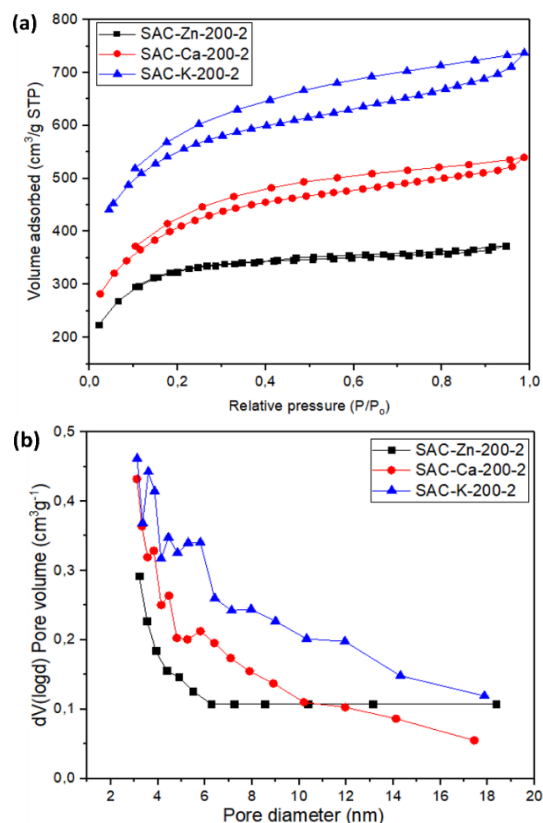

Figure 3. (a) N_2 adsorption-desorption isotherm curves and (b) pore size distribution of activated carbon with various activators

According to Figure 3b, the pore size distributions (PSD) of SAC prepared using different activators show that all the samples have a wide PSD, mainly centered at 2 to 18 nm; hence this result is charming and demonstrates a profoundly mesoporous carbon structure. Foo and Hameed (2011a) mentioned a typical pore size of 21.44 nm in initiated carbon produced from pistachio nutshells using microwave-instigated substance (KOH) activation. Additionally, activated carbon made from rice husk as a feedstock was reported to have mean pore diameters of 34.14 nm and 26.89 nm (Foo and Hameed, 2011b). Figure 3b shows that activator type affects the volume of the pore size distribution formed.

Figure 4 shows the effect of hydrothermal temperature and the ratio of activator to biomass on adsorption volume and PSD on activated carbon. The upgrade in hydrothermal temperature generally increases the volume of N_2 adsorbed. Also, the surface area of activated carbon tends to elevate with increasing hydrothermal temperature due to the formation of volatiles during heating, increasing this

product's porosity. The activators involved in the hydrothermal process remove the oxygen and hydrogen content in the biomass, then form water, thereby increasing the porosity and surface area of the activated carbon after passing through the activation (Jain et al., 2015).
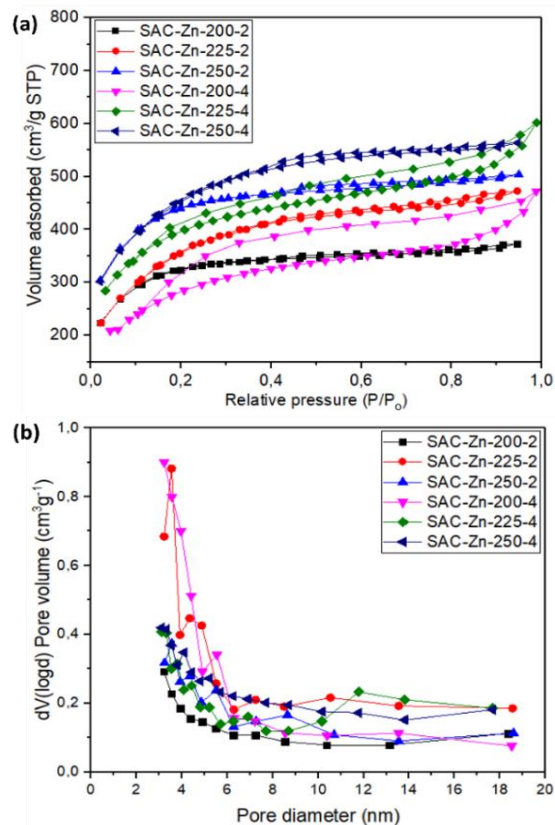

Figure 4. (a) N_2 adsorption-desorption isotherm curve with $ZnCl_2$ and (b) pore size distribution of activated carbon with different hydrothermal temperatures and activator ratio

Figure 4 also shows that the ratio of activator to biomass influences the volume of nitrogen adsorption. The extension in the balance of $ZnCl_2$ expanded the surface space of the enacted carbon. It has been indicated that extending the ratio as mentioned above constructs the textural properties (surface locale and pore volume) attributed to growing the drawing effect of the activator on the biochar surface, leading to mesopores production from the micropores (Wu et al., 2017). Conversely, the $CaCl_2$ and KOH showed the inverse; in particular, the overhaul in the proportion of activator diminished the surface space of the enacted carbon. Impregnation ratios excessively huge for specific activators harm the framed pore structure, consequently decreasing the surface area of activated carbon.

Crystalline structure characterization

X-ray diffraction (XRD) was used to decide the crystallographic structure of the samples. The XRD structure for the three activated carbon prepared with different activators can be seen in Figure 5. The XRD

pattern for the three samples showed a structured hexagonal mesoporous layout (Lu et al., 2017). The enormous top at $2\theta = 26.03^\circ$ (C(002)) in Figure 5 is related to the amorphous carbon layer. The frail and expansive C(100) top at $2\theta = 43^\circ$ (C(100)) was ascribed to the pivot of the graphitic structure (Liu et al., 2016). The peaks of C002 and C100 of the samples with KOH had the highest intensity. This indicates the

KOH plays the best role in forming the amorphous structure and the degree of graphitization of the activated carbon. However, the XRD pattern for the three sample tests is similar, indicating that various activators do not significantly affect the immediate changes in the activated carbon (Hossain et al., 2018).
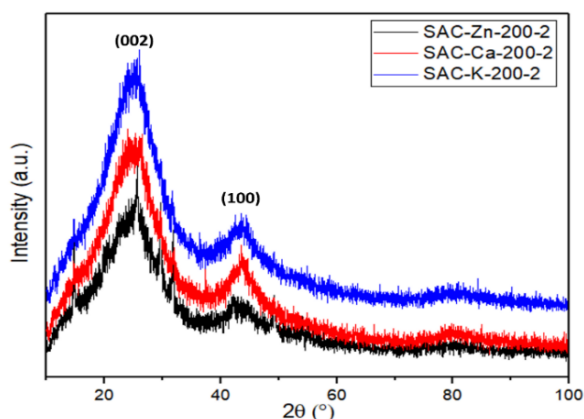

Figure 5. XRD patterns of the *Sargassum* sp.-derived activated carbon with various activators

Multilevel Factorial Design Analysis
Effect of the factors on SAC yield

The multilevel factorial experiment with the factors and levels shown in Table 1 had 18 trials. According to Table 3, the experimental results were dissected using statistical software MINITAB 19 to assess the impact of working variables involving statistical factors and plots (Pareto, probability standard effects, main effects, and interaction plots). Furthermore, activated carbon yield was expressed in weight percent, then analysis of variance (ANOVA) was employed to decide the collaborations between main factors' interactions. The main effects to yield value were recognized as dependent on the *P*-value with $\alpha > 95\%$ confidence level (Özbay et al., 2013; Secula et al., 2013).

Analysis of variance is a statistical method for dividing total variation into components, each of which is linked to a different cause (Safa and Bhatti, 2011; Özbay et al., 2013). The interaction effects are also easily computed and tested using the usual ANOVA; hence the yield results can be seen in Table 4. Based on the degree of freedom (DF), the sum of the squares (SS), mean of squares (MS), F-values, and P-values in table 4, factor *A* and *A*C* interaction (type of activator with its dose) have a p-value of less than 0.05. This indicates that the yield model has a

significant response to changes in the nature of the activator.

The yield values obtained from 18 experiments were in the range of 5.2 & 17.2%, and as a response variable to factor and level, it is expressed by the following equation:

$$
\begin{aligned}
Y_1 = {} & 16.094 + 0.922A_1 + 7.172A_2 - 8.094A_3 \\
& + 0.456B_1 + 0.128B_2 - 0.328B_3 - 1.017C_1 \\
& + 1.017C_2 + 0.38A_1B_1 + 0.66A_1B_2 \\
& - 1.04A_1B_3 + 1.38A_2B_1 - 1.74A_2B_2 \\
& + 3.217A_2C_1 - 3.217A_2C_2 - 1.35A_3C_1 \\
& + 1.35A_3C_2 + 0.233B_1C_1 - 0.233B_1C_2 \\
& - 0.25B_2C_1 + 0.25B_2C_2 + 0.17B_3C_1 \\
& - 0.17B_3C_2
\end{aligned}
\tag{2}
$$

Where Y_1 is the response or SAC yield, *A* is three types of activator ($ZnCl_2$, $CaCl_2$, & KOH), *B* is a variation of temperature (200, 225, & 250°C), and *C* is activator ratio (2 & 4).

A Pareto diagram is used to decide the greatness and significance of the impact; therefore, the chart shows the outright worth of the expected effect from the most significant impact to the least. The outline also plots reference lines to indicate the genuinely tremendous results. The reference line for factual importance relies upon the importance level (signified by α or alpha). The Pareto chart of standardized effects on yield of SAC can be seen in figure 6, where the bars represent factors *A* and *A*C*, which crosses the reference line at 2.776. This means activator type (*A*) and interaction with its ratio (*A*C*) are statistically significant at the 0.05 level in the yield model.

Table 4. Analysis of variance (ANOVA) for the yield of SAC

Source	DF	SS	MS	F-Value	P-Value
Model	13	844.916	64..994	12.61	0.013
Linear	5	727.461	145.492	28.23	0.003
A	2	706.868	353.434	68.58	0.001
B	2	1.988	0.994	0.19	0.832
C	1	18.605	18.605	3.61	0.130
2-Way Interactions	8	117.456	14.682	2.85	0.163
A*B	4	22.829	5.707	1.11	0.462
A*C	2	93.923	46.962	9.11	0.032
B*C	2	0.703	0.352	0.07	0.935
Error	4	20.613	5.153		
Total	17	865.529			

The main effect and interaction plots can be seen in Figure 7, highlighting the influences on the yield. With the addition of KOH, the average yield value obtained begins to decrease (Figure 7a).

The use of the $CaCl_2$ activator had the opposite, increasing effect, observable from the interaction plot (Figure 7b) and the ANOVA test (Table 4)

$$Y_2 = 1140.4 + 185.4A_1 - 371.9A_2 + 186.6A_3$$
$$- 60.3B_1 + 14.4B_2 + 45.9B_3 - 107.4C_1$$
$$- 107.4C_2 - 75A_1B_1 - 55A_1B_2 + 129A_1B_3$$
$$+ 182A_2B_1 + 109A_2B_2 - A_2B_3 - 107A_3B_1 \quad (3)$$
$$- 54A_3B_2 + 161A_3B_3 - 177.3A_1C_1$$
$$+ 177.3A_1C_2 + 175.7A_2C_1 - 175.7A_2C_2$$
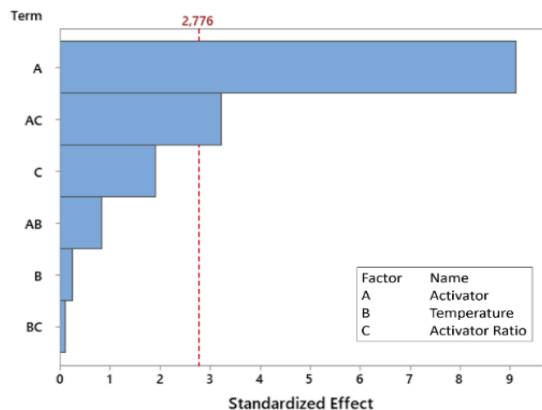$$+ 1.6A_3C_1 - 1.6A_3C_2$$

Figure 6. Pareto chart of standardized effects with yield as a response, at $\alpha = 0.05$
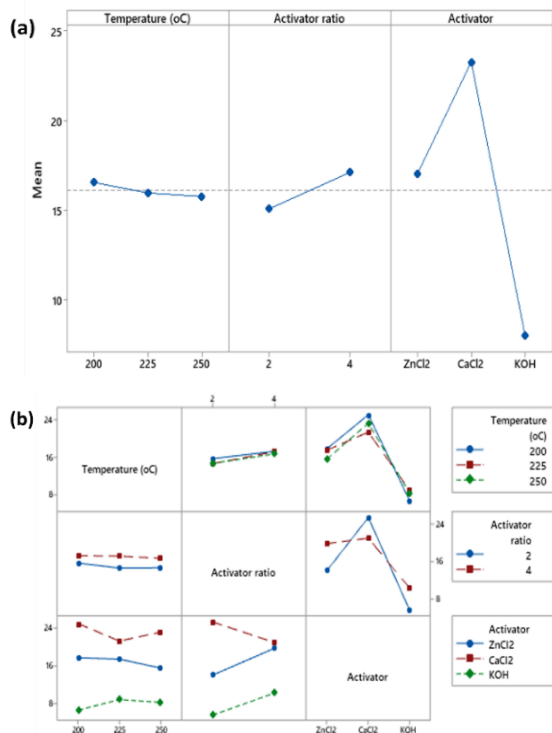

Figure 7. (a) Main effects and (b) interactions plots pointing out the effects on yield.

According to the ANOVA test, the interaction between activator type and dose (AC) was statistically significant at the 95.0 % confidence level. Activator type is more critical at a low ratio for $CaCl_2$, which is due to the elimination of hydrogen and oxygen from the biomass using this agent, leading to a relatively

low loss of volatile matter tars (Titirici et al., 2015). Meanwhile, according to Jain et al. (2014), the results of the biomass-based precursor carbonization process ranged from 20-30 %wt, causing the yield value of this study to be in line with the literature.

Effect of the factors on the surface area of SAC

The SAC's surface area was calculated using the BET method from the N_2 adsorption-desorption data of the sample. The value of SAC's BET-specific surface area (S_{BET}) was in the range of 415 and 1799 m^2/g. The following equation expresses S_{BET} as a response variable to factor and level:
where Y_2 is the response of S_{BET}.

Table 5. Analysis of variance (ANOVA) for the S_{BET} of SAC

Source	DF	Adj SS	Adj MS	F-Value	P-Value
Model	11	2251.989	20.726	2.69	0.118
Linear	5	1488.563	297.713	3.92	0.063
A	2	1245.088	622.544	8.19	0.019
B	2	35.677	17.839	0.23	0.798
C	1	207.798	207.798	2.73	0.149
2-Way Interactions	6	763.426	127.238	1.67	0.274
A*B	4	389.577	97.394	1.28	0.374
A*C	2	373.849	186.924	2.46	0.166
Error	6	456.242	76.040		
Total	17	2708.230			

The analysis of variance (ANOVA) value can be seen in Table 5, which shows that just factor *A* has a p-value of less than 0.05, meaning the S_{BET} model has a significant response to changes in the type of activator.
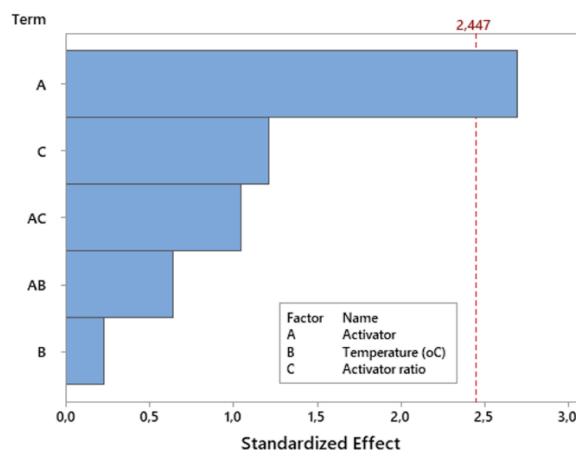

Figure 8. Pareto chart of standardized effects with S_{BET} as a response, at $\alpha = 0.05$

The Pareto chart of standardized effects on S_{BET} of SAC can be seen in figure 8, where the bars represent the factors and *A* crosses the reference line at 2.447. Therefore, the type of activator (*A*) is statistically significant at the 0.05 level of the model.
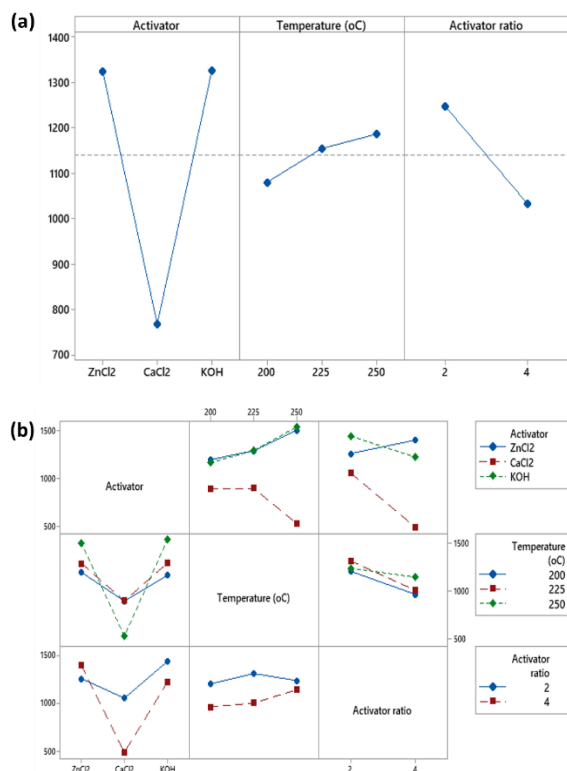
Figure 9. (a) Main effects and (b) interaction plots indicating the effects on S_{BET}.

The main effect and interaction plots of the factors can be seen in figure 9; hence 9a shows the activator and its ratio, as well as temperature, provide different mean responses to the variation of the experimental factors. Also, according to Figure 9b, there is a change in response to factor and level interactions. However, the primary factor test and interaction with the Pareto graph and ANOVA above indicated that only the activator type was statistically significant in changing the response of S_{BET}. Dolores et al. (2013) stated that the formation of activated carbon depends on the type of biomass source and the preparation stage. In contrast, the construction of activated carbon porosity significantly relies on the activation stage. The preparation stage is the hydrothermal carbonization of *Sargassum* sp. with variations in activator type and ratio, plus hydrothermal temperature. In the activation process, temperature variations are not performed, meaning hydrothermal temperature has no significant effect on the activated carbon porosity (Hossain et al., 2018).

CONCLUSIONS

Sargassum sp.-derived active carbon (SAC) was successfully produced using hydrothermal carbonization and the CO_2 activation process. The hydrothermal processes that were carried out involve variables of activator type, activator ratio, and hydrothermal temperature. Meanwhile, the pyrolysis process was carried out at a constant temperature of 800 ᵒC. Hydrothermal carbonization and pyrolysis activation increased the carbon content in hydrochar

and activated carbon from 37.8% and 79.5%, respectively, from the raw material of 21.11%. Meanwhile, the O/C atomic ratio fell to 1.2% and 0.29%, respectively, from 2.68%. FTIR analysis showed that the type and intensity of the functional groups on activated carbon were significantly affected by the type of activator. However, the effect of temperature on the functional groups was not significant. Morphological analysis of activated carbon showed that pores were clearly formed on the material's surface.

Meanwhile, the crystallographic analysis showed that all activated carbon samples had an amorphous structure with a partial graphitic structure. The yield of activated carbon is significantly influenced by the type of activator and the interaction between the type of activator and the ratio of activator to raw materials. The highest yield of activated carbon was obtained at 27.5 percent for the SAC-Ca-250-2 sample. The specific surface area (S_{BET}) of activated carbon was significantly affected by the type of activator, with the highest specific surface area for various activators being 1552, 1368, and 1799 m²/g, respectively, for SAC-Zn-250-4, SAC-Ca-225- 2, and SAC-K-250-2. The SAC product has a mesoporous structure with a pore size distribution between 2.16-18 nm. The research findings show that the hydrothermal carbonization process by applying an activator followed by the pyrolysis activation process can be a promising method to produce high-quality activated carbon.

REFERENCES

Ali, I., and Bahadar, A., (2017), Red Sea seaweed (*Sargassum* spp.) pyrolysis and its devotilization kinetics, *Algal Research*, 21, pp. 89–97.

Brown, A. E., Finnerty, G. L., Camargo-Valero, M. A. and Ross, A. B., (2020), Valorisation of macroalgae via the integration of hydrothermal carbonization and anaerobic digestion, *Bioresource Technology*, 312, pp. 123539.

Cai, J., Lovatelli, A., Aguilar-Manjarrez, J., Cornish, L., Dabbadie, L., Desrochers, A., Diffey, S., Gamaro, E.G., Geehan, J., Hurtado, A., Lucente, D., Mair, G., Miao, W., Potin, P., Przybyla, C., Reantaso, M., Roubach, R., Tauati, M. and Yuan, X., (2021), *Seaweeds and Microalgae: an Overview for Unlocking Their Potential in Global Aquaculture Development*, FAO Fisheries and Aquaculture Circular No. 1229, Rome: FAO.

Dolores, L. C., Juan, P. M. L., Falco, C., Titirici, M. M. and Diego, C. A., (2013), Porous Biomass-Derived Carbons: Activated Carbons, in Titirici, M.-M. (ed.) *Sustainable Carbon Materials from Hydrothermal Processes*. First Edition, The United Kingdom: John Wiley & Sons, Ltd, pp. 75–100.

Foo, K. Y., and Hameed, B. H., (2011a), Preparation and characterization of activated carbon from pistachio nut shells via microwave-induced chemical activation, *Biomass and Bioenergy*, 35(7), pp. 3257–3261.

Foo, K. Y. and Hameed, B. H., (2011b), Utilization of rice husks as a feedstock for preparation of activated carbon by microwave-induced KOH and K_2CO_3 activation, *Bioresource Technology*, 102(20), pp. 9814–9817.

Gao, P., Zhou, Y., Meng, F., Zhang, Y., Liu, Z., Zhang, W., and Xue, G., (2016), Preparation and characterization of hydrochar from waste eucalyptus bark by hydrothermal carbonization, *Energy*, 97, pp. 238–245.

He, Y., Zhang, Y., Li, X., Lv, Z., Wang, X., Liu, Z. and Huang, X., (2018), Capacitive mechanism of oxygen functional groups on carbon surface in supercapacitors, *Electrochimica Acta*, 282, pp. 618–625.

Hoekman, S. K., Broch, A., and Robbins, C., (2011), Hydrothermal carbonization (HTC) of lignocellulosic biomass, *Energy and Fuels*, 25(4), pp. 1802–1810.

Hossain, M., Wu, W., Xu, W., Chowdhury, M., Jhawar, A., Machin, D. and Charpentier, P., (2018), High-Surface-Area Mesoporous Activated Carbon from Hemp Bast Fiber Using Hydrothermal Processing, *Journal of Carbon Research*, 4(3), p. 38.

Inagaki, M. and Kang, F., (2014), Fundamental Science of Carbon Materials, in *Materials Science and Engineering of Carbon: Fundamentals*. Elsevier Inc., pp. 17–217.

Jain, A., Balasubramanian, R. and Srinivasan, M. P., (2015), production of high surface area mesoporous activated carbons from waste biomass using hydrogen peroxide-mediated hydrothermal treatment for adsorption applications, *Chemical Engineering Journal*, 273, pp. 622–629.

Jain, A., Balasubramanian, R. and Srinivasan, M. P., (2016), Hydrothermal conversion of biomass waste to activated carbon with high porosity: A review, *Chemical Engineering Journal*, 283(December 2017), pp. 789–805.

Choline Chloride (ChCl) Catalyst, *International Journal of Renewable Energy Development*, 11(2), pp. 403–412.

Jain, A., Jayaraman, S., Balasubramanian, R. and Srinivasan, M. P., (2014), Hydrothermal pretreatment for mesoporous carbon synthesis: Enhancement of chemical activation, *Journal of Materials Chemistry A*, 2(2), pp. 520–528.

Kim, S. S., Ly, H. V., Kim, J., Choi, J. H. and Woo, H.C., (2013), Thermogravimetric characteristics and pyrolysis kinetics of Alga *Sagarssum* sp. biomass, *Bioresource Technology*, 139, pp. 242–248.

Li, D., Chen, L., Zhang, X., Ye, N. and Xing, F., (2011), Pyrolytic characteristics and kinetic studies of three kinds of red algae, *Biomass and Bioenergy*, 35(5), pp. 1765–1772.

Liu, F., Liu, L., Li, X., Zeng, J., Du, L. and Liao, S., (2016), Nitrogen self-doped carbon nanoparticles derived from spiral seaweeds for oxygen reduction reaction, *RSC Advances*, 6(33), pp. 27535–27541.

Lu, Y., Zhang, S., Yin, J., Bai, C., Zhang, J., Li, Y., Yang, Y., Ge, Z., Zhang, M., Wei, L., Ma, M., Ma, Y. and Chen, Y., (2017), Mesoporous activated carbon materials with ultrahigh mesopore volume and effective specific surface area for high-performance supercapacitors, *carbon*, 124, pp. 64–71.

Özbay, N., Yargiç, A. Ş., Yarbay-Şahin, R. Z. and Önal, E., (2013), Full factorial experimental design analysis of reactive dye removal by carbon adsorption, *Journal of Chemistry*, 2013.

Perez-Salcedo, K. Y., Ruan, S., Su, J., Shi, X., Kannan, A. M. and Escobar, B., (2020), Seaweed-derived KOH activated biocarbon for electrocatalytic oxygen reduction and supercapacitor applications, *Journal of Porous Materials*, 27(4), pp. 959–969.

Pintor, M. J., Jean-Marius, C., Jeanne-Rose, V., Taberna, P. L., Simon, P., Gamby, J., Gadiou, R. and Gaspard, S., (2013), Preparation of activated carbon from Turbinaria turbinata seaweeds and its use as supercapacitor electrode materials, *Comptes Rendus Chimie*, 16(1), pp. 73–79.

Pourhosseini, S. E. M., Norouzi, O., and Naderi, H. R., (2017), Study of micro/macro ordered porous carbon with an olive-shaped structure derived from Cladophora glomerata macroalgae as efficient working electrodes of supercapacitors, *Biomass and Bioenergy*, 107, pp. 287–298.

Rustamaji, H., Prakoso, T., Rizkiana, J., Devianto, H., Widiatmoko, P. and Guan, G., (2022a), Synthesis and Characterization of Hydrochar and Bio-oil from Hydrothermal Carbonization of *Sargassum* sp. using

Rustamaji, H., Prakoso, T., Devianto, H., Widiatmoko, P., Saputera W. H., (2022b), Urea nitrogenated mesoporous activated carbon derived

from oil palm empty fruit bunch for high-performance supercapacitor, *Journal of Energy Storage*, 52 104724.

Safa, Y. and Bhatti, H. N., (2011), Adsorptive removal of direct textile dyes by low-cost agricultural waste: Application of factorial design analysis, *Chemical Engineering Journal*, 167(1), pp. 35–41.

Saha, N., Sabab, A., and Reza, T., (2019), Effect of hydrothermal carbonization temperature on pH, dissociation constants, and acidic functional groups on hydrochar from cellulose and wood. *Journal of Analytical and Applied Pyrolysis*, 137, pp. 138-145.

Saleh, H. and Sebastian, E., (2020), Seaweed Nation : Indonesia's new growth sector, 2, pp. 1–19.

Secula, M. S., Cretescu, I., Cagnon, B., Manea, L. R., Stan, C. S. and Breaban, I. G., (2013), Fractional factorial design study on the performance of GAC-enhanced electrocoagulation process involved in color removal from dye solutions, *Materials*, 6(7), pp. 2723–2746.

Smith, A. M. and Ross, A. B., (2016), production of bio-coal, bio-methane and fertilizer from seaweed via hydrothermal carbonization, *Algal Research*, 16, pp. 1–11.

Sun, P., Zhang, B., Zeng, X., Luo, G., Li, X., Yao, H. and Zheng, C., (2017), Deep study on effects of activated carbon's oxygen functional groups for elemental mercury adsorption using temperature-programmed desorption method, *Fuel*, 200, pp. 100–106.

Tekin, K., Karagöz, S. and Bektaş, S., (2014), A review of hydrothermal biomass processing, *Renewable and Sustainable Energy Reviews*, 40, pp. 673–687.

Zhang, Z., Wang, K., Atkinson, J. D., Yan, X., Li, X., Rood, M. J. and Yan, Z., (2012), Sustainable and hierarchical porous Enteromorpha prolifera based carbon for CO2 capture, *Journal of Hazardous Materials*, 229–230, pp. 183–191.

Titirici, M. M., White, R.J., Brun, N., Budarin, V.L., Su, D.S., Del Monte, F., Clark, J.H. and MacLachlan, M.J., (2015), Sustainable carbon materials, Chemical Society Reviews, 44(1), pp. 250–290.

Titirici, M. M., (2013), Sustainable carbon materials from hydrothermal processes, John Wiley & Sons, United Kingdom, pp. 64-65

Wang, T., Zhai, Y., Zhu, Y., Lia, C., and Zeng, G., (2018), A review of the hydrothermal carbonization of biomass waste for hydrochar formation: Process conditions, fundamentals, and physicochemical properties, Renewable and Sustainable Energy Reviews, 90, pp. 223–247.

Wu, Y., Cao, J. P., Zhao, X. Y., Hao, Z. Q., Zhuang, Q. Q., Zhu, J. S., Wang, X. Y. and Wei, X. Y., (2017), Preparation of porous carbons by hydrothermal carbonization and KOH activation of lignite and their performance for electric double-layer capacitor, Electrochimica Acta, 252, pp. 397–407.

Xu, Q., Qian, Q., Quek, A., Ai, N., Zeng, G. and Wang, J., (2013), Hydrothermal Carbonization of Macroalgae and the Effects of Experimental Parameters on the Properties of Hydrochars, ACS Sustainable Chemistry & Engineering, 1, pp. 1092–1101.

Yang, S. Y., Chang, K. H., Huang, Y. L., Lee, Y. F., Tien, H. W., Li, S. M., Lee, Y. H., Liu, C. H., Ma, C. C. M. and Hu, C. C., (2012), A powerful approach to fabricate nitrogen-doped graphene sheets with high specific surface area, Electrochemistry Communications, 14(1), pp. 39–42.

Zeng, G., Lou, S., Ying, H., Wu, X., Dou, X., Ai, N. and Wang, J., (2018), Preparation of Microporous Carbon from Sargassum horneri by Hydrothermal Carbonization and KOH Activation for CO2 Capture, Journal of Chemistry, 2018, p. 11.